GUANGZHOU UNIVERSITY

GMSS – A Software Package for Implementing Stochastic Ground Motion Simulations: Version 2.0

By

Yuxiang Tang[1]

19 September 2021

[1] Guangzhou University, Guangzhou, Guangdong, China. Email: tangyuxiang56@gmail.com

Table of Contents

Disclaimer: This program is distributed for academic research sharing purposes only. There is no warranty, expressed or implied, from any individual (including the author Yuxiang Tang) or any institutions or affiliations. Any potential end-users should use this program with caution.

GMSS2.0 is available at: https://github.com/Y-Tang99/GMSS2.0

1. Introduction

This report contains a fundamental principle and implementation instructions of GMSS2.0, which is an enhanced software package for stochastic finite-fault ground motion simulation. The approach of generating accelerograms by the computer through the use of band-limited random signals to represent seismic waves radiated from the source of the earthquake along with modifications of the frequency contents of the radiated waves along their travel path is widely used in engineering seismology as well as in civil and structural engineering. The methodology as described for simulating ground motions is known as stochastic simulations. The frequency content of the simulated accelerograms is controlled by the seismological model. This study is mainly concerned with stochastic simulations of the seismological model for the generation of accelerograms (Boore & Joyner, 1991; Joshi, et al. 1999; Lam, et al. 2000). Many Ground motion models that have been developed for tectonically stable areas are based on this methodology (Boore, 2003).

The stochastic simulation method (or stochastic model) refers to a method of describing the seismic source and path in a partially stochastic, rather than a completely deterministic way (Boore, 2003). The essence of this method described in this study is based on the combination of seismological models (defining the Fourier amplitude of ground motions) with the engineering notion that ground motions are generally random at high frequencies (Hanks & McGuire, 1981). The essential ingredient for the stochastic simulation method is the seismological model that contains the physics of the earthquake process and wave propagation.

The translation of a seismological model for simulating accelerograms, or for the development of a GMPE, requires a computer software such as SMSIM (Boore, 2003) or GENQKE (Lam, et al. 2000) for undertaking the simulations (for point source), and EXSIM (Boore, 2009a) (for finite-fault source). Proper use of such simulation software requires a good understanding of stochastic simulations and seismological models to avoid misuse of the software. The author favors guiding how to simulate accelerograms on a generic analytical platform using MATLAB or Python, to assist designers and fellow researchers as opposed to offering the program (SMSIM or EXSIM) as a "black box" tool.

The MATLAB package introduced herein is called “GMSS”, which is short for *Ground Motion Simulation System*. The package contains two different types of programs. The first type (named GMSS2SS) is based on a wrapper script running in MATLAB and is designed for a single scenario (**M** - **R** combination) simulation. For this type, each step of computation is illustrated in a detailed way, and each parameter value is shown in the workspace in MATLAB to assist the end-users to learn how GMSS2.0 is programmed. The second type (GMSS2MS) is also based on wrapper script running in MATLAB and is designed for multiple-scenario simulation. The use of this type can facilitate the engineering applications that accelerograms of multiple scenarios are required, e.g. the development of Ground Motion Model (GMMs). Detailed information can be found in the following sections.

2. *Seismological Models Used in GMSS2.0*

The basic idea of GMSS2.0, which follows the EXSIM_DMB (Boore, 2009a) and EXSIM12 (Atkinson and Assatourians, 2015), is to divide the fault source into a number of subfaults, and each subfault is regarded as a point source. The seismological model (which is deterministic) is the most important ingredient in the stochastic method. The basic functional form of a seismological model for the ij^{th} subfault source can be expressed as Eq. (1):

$$FA(M_{0ij}, R_{ij}, f) = E(M_{0ij}, f) * G(R_{ij}) * Ae(f, R_{ij}) * Am(f) * An(f) \quad (1)$$

where $FA(M_{0ij}, R_{ij}, f)$ is the target Fourier spectrum; $E(M_{0ij}, f)$ is the source factor; $G(R_{ij})$ is the geometric spreading (attenuation) factor; $Ae(f, R_{ij})$ is the anelastic whole path attenuation factor; $Am(f)$ is the upper-crust amplification factor; $An(f)$ is the upper-crust attenuation factor; M_{0ij} is defined as the seismic moment in the unit of dyne-cm; f is the frequency of the ground motion in Hz; R_{ij} is the distance between the source and the site in the unit of km.

2.1 Source factors

Source factors that have been developed to date based on the notion of a "point source" have been reported in the literature (Atkinson & Boore, 1995; Atkinson, 2004; Atkinson & Boore, 2014; Boore, 1983; Brune, 1970). A Point Source Model considers the source of an earthquake as a point from which seismic waves are radiated. If the source of the earthquake is large enough that cannot be regarded as a "point", the point source model may not be capable of representing all the source features of the real earthquake source, and some researchers put forward the finite fault source model. The finite fault model considers the earthquake generating source as a fault that is made up of several sub-faults and each sub-fault can be treated as a point source (Zeng, et al. 1994).

Following Brune's source model, the most commonly accepted source in FAS is represented by the single-corner frequency source factor for a single subfault (Brune, 1970), which is defined by Eq. (2):

$$E_{ij} = (2\pi f)^2 \frac{CM_{0ij}}{1+(f/f_{0ij})^2} S_{ij} \quad (2)$$

in which, f is the frequency, C is the mid-crust scaling factor; M_{0ij}, f_{0ij} and S_{ij} are seismic moment, corner-frequency, and scaling factor for the ij^{th} subfault, respectively.

In Eq. (2), C is the mid-crust scaling factor as defined by Eq. (3) (Atkinson, 1993):

$$C = \frac{R_p F V}{4\pi\rho_0\beta_0^3 R_0} \quad (3)$$

where $R_0 = 1$ km; R_p is the radiation pattern factor (= 0.55), usually averaged over a suitable range of azimuths and take-off angles; F is the free surface amplification factor (= 2.0), and the value of 2.0 strictly speaking is only valid for shear-waves; V represents the partitioning

factor of total shear-wave energy into two horizontal components (= $1/\sqrt{2}$); ρ_0 and β_0 are the density and shear-wave velocity (SWV) in the vicinity of the source, and the unit is g/cm^3 and km/s respectively in this study.

In Eq. (2), M_{0ij} can be determined using Eq. (4):

$$M_{0ij} = \frac{M_0 W_{ij}}{\sum_{l=1}^{nl} \sum_{w=1}^{nw} W_{lw}} \tag{4}$$

where M_0 is the total seismic magnitude and W_{ij} is the relative slip weight of the ij^{th} subfault; nl and nw is the number of subfaults along strike and down dip of the finite fault, respectively.

The total seismic moment M_0 can be expressed in terms of the moment magnitude which is given by Eq. (5) (Hanks & Kanamori, 1979):

$$M = 0.67\, log(M_0) - 10.7 \tag{5}$$

which is the same given by (Boore, et al. 2014) and shown as Eq. (6):

$$\log(\mathrm{M_0}) = 1.5\mathrm{M} + 16.05 \tag{6}$$

In Eq. (2), f_{0ij} is defined by Eq. (7) (Tang, 2022a):

$$f_{0ij} = 4.9 \times 10^6 \beta_0 \left(\frac{\Delta\sigma}{p \times M_0}\right)^{1/3} \tag{7a}$$

$$f_{0ij} = 4.2 \times 10^6 yz\beta_0 \left(\frac{\Delta\sigma}{p \times M_0}\right)^{1/3} \tag{7b}$$

Eq. (7a) is the rupture velocity independent corner-frequency model, and it is used by currently distributed EXSIM; while Eq. (7b) is the rupture velocity-dependent corner-frequency model, and the detailed derivation procedures of this model can be found in the BSSA article (Tang, 2022a); y in Eq. (7b) represents the ratio of rupture velocity (V_{rup}) and source shear-wave velocity (β_0), and z is the parameter defining the strength of high-frequency radiation. In Eq. (7), p is the parameter defining the pulsing percentage, and it is determined by Eq. (8):

$$p = \begin{cases} N_R/N, & N_R < N \times pp \\ pp, & N_R \geq N \times pp \end{cases} \tag{8}$$

where N_R is the cumulative number of pulsing subfaults, which is determined by a parameter that gives the percentage of total rupture area (pp); N is the total number of subfaults.

In Eq. (2), S_{ij} is the scaling factor introduced by Boore (2009a), which is used to eliminate the influences of subfault size on spectral amplitude at lower frequencies due to the incoherent summation, and it can be calculated by Eq. (9):

$$S_{ij} = CS_{ij} \frac{1+(f/f_{0ij})^2}{1+(f/f_{0effij})^2} \tag{9a}$$

where

$$CS_{ij} = \sqrt{N}/H_{ij} \tag{9b}$$

$$f_{0effij} = f_{0ij}/\sqrt{CS_{ij}} \tag{9c}$$

In Eq. (7), if $f \to 0$, $S_{ij} \to CS_{ij}$; and if $f \to \infty$, $S_{ij} \to 1$.

H_{ij} in Eq. (9b) is the scaling factor used to eliminate subfault size influences on Fourier amplitude at high frequencies. The updated H_{ij} based on acceleration (rather than velocity) is expressed by Eq. (10a), and the simplified H_{ij} can be expressed by Eq. (10b) (Boore, 2009a):

$$H_{ij} = (M_0/M_{0ij}) \times \sqrt{\sum(\frac{f_0^2 f}{f_0^2+f^2})^2 \Big/ N \sum(\frac{f_{0ij}^2 f}{f_{0ij}^2+f^2})^2} \tag{10a}$$

$$H_{ij} = \sqrt{N}\left(\frac{f_0}{f_{0ij}}\right)^2 \tag{10b}$$

where f_0 is the corner-frequency for the whole fault, which can be determined from Eq. (11):

$$f_0 = 4.9 \times 10^6 \beta_0 \left(\frac{\Delta\sigma}{M_0}\right)^{1/3} \tag{11a}$$

$$f_0 = 4.2 \times 10^6 yz\beta_0 \left(\frac{\Delta\sigma}{M_0}\right)^{1/3} \tag{11b}$$

The rest components in Eq.(1) will be introduced in sections 2.2 and 2.3.

The final time series of the whole fault source can be computed using Eq. (12):

$$A(t) = \sum_{i=1}^{nl}\sum_{j=1}^{nw} H_{ij} \times Y_{ij}(t + \Delta t_{ij} + \Delta T_{ij}) \tag{12}$$

where $A(t)$ is the total time series of the seismic signal at a site; $Y_{ij}(t)$ is the signal of the ij^{th} subfault, which is obtained from inverse Fourier transform of FA_{ij} shown in Eq. (1); Δt_{ij} is the delay time of the ij^{th} subfault along the path; ΔT_{ij} is the delay time for ij^{th} subsource and is proportional to the source duration of the subfault (T_{0ij}).

2.2 Path factors

Path factor, or attenuation factor, is used to describe the spreading characteristics of seismic waves radiated from sources. For most applications, the path effect is represented by simple functions that account for geometric spreading, intrinsic and scattering attenuation (also known as anelastic attenuation), and the general increase of duration with distance due to wave propagation and scattering (considered by path duration) (Boore, 2003). Some examples are given in Table 1 (Boore, 2015) for the path functions (containing geometric spreading and whole path anelastic attenuation factors). Figs. 1 and 2 are the two examples for showing different geometric spreading and anelastic attenuation models, the detailed parameter values for the example attenuation models are shown in Table 1.

$G(R_{ij})$ in Eq. (1) is given by the subfault distance and mainly accounts for the regional geometric attenuation pattern of the seismic wave along the path. G_{ij} does not have a fixed functional format and is a region-dependent parameter.

$Ae(f, R_{ij})$ in Eq. (1) is expressed by Eq. (13):

$$Ae(f, R_{ij}) = \exp\left(\frac{-\pi f R_{ij}}{Q\beta_0}\right) \quad (13)$$

where Q is the regional quality factor and is inversely related to anelastic attenuation.

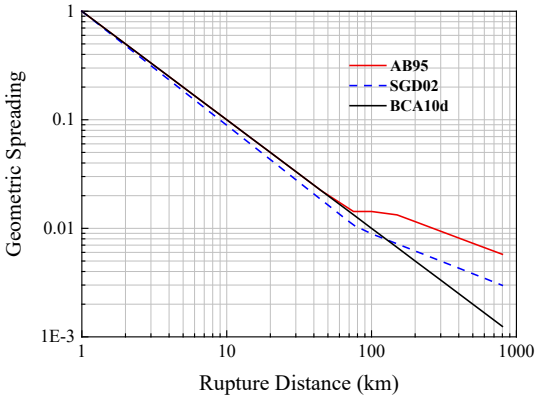

Figure 1. Sample of geometric spreading models

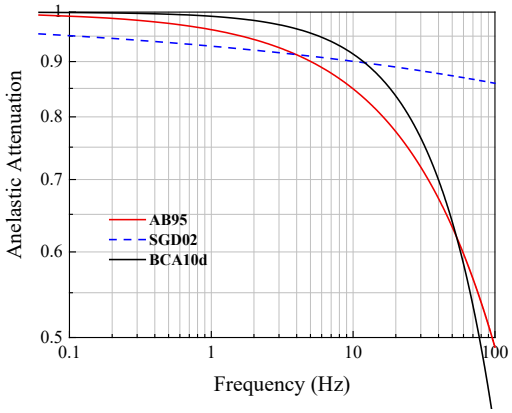

Figure 2. Sample of anelastic attenuation models

It should be noted that if the path functions are determined from recorded/simulated data, it is important to balance the trade-off effects between geometric spreading and anelastic attenuation and the fitting with the data for both. It is important to keep the consistency of geometric spreading and anelastic attenuation functions in practical applications (they need to be adopted from the same seismological model).

Another important part of the path factor is the distance-dependent ground motion duration. Because the seismological model itself is not related to the duration factor, this will be discussed in Section 3.

Table 1. Example attenuation models for NGA-East

Geometric spreading functions	" R"	" Q"	Applicable range	Model and Reference
$R \le 70$, $(R) = R^{-1}$; $70 \le R \le 130$, $(R) = 70^{-1} * (\frac{R}{70})^{0}$; $R > 130$, $(R) = 70^{-1} * 130^{0} * (\frac{R}{130})^{-0.5}$	$R = R_{hyp}$	$Q(f) = 680f^{0.36}$	$4 \le \mathbf{M} \le 7.25$ $10 \le \mathbf{R} \le 500$ $0.5 \le f \le 20$	**AB95** (Atkinson & Boore, 1995)
$R \le 80$, $(R) = R^{-(1.0296-0.0422(M-6.5))}$ $R > 80$, $(R) = 80^{-(1.0296-0.0422(M-6.5))} * R^{-0.5*(1.0296-0.0422(M-6.5))}$	$R = R_{hyp}$	$Q(f) = 351f^{0.84}$	$4.5 \le \mathbf{M} \le 8.5$ $1 \le \mathbf{R} \le 400$ $0.1 \le f \le 100$	**SGD02** (Silva, et al.2002)
$R \le 70$, $(R) = R^{-1.3}$ $70 \le R \le 140$, $(R) = 70^{-1.3} * (\frac{R}{70})^{0.2}$; $R > 140$, $(R) = 70^{-1} * 140^{0.2} * (\frac{R}{140})^{-0.5}$	$R = R_{hyp}$	$Q(f) = max\,(1000, 893f^{0.3}$	$4.4 \le \mathbf{M} \le 6.8$ $10 \le \mathbf{R} \le 800$ $0.05 \le f \le 20$	**A04** (Atkinson, 2004)
$(R) = R^{-1}$, *for all* R	$R = (R_{hyp}{}^2 + h_{FF}{}^2)^{0.5}$, $h_{FF} = 10^{-0.405+0.235M}$	$Q(f) = 2850$	$4.4 \le \mathbf{M} \le 6.8$ $10 \le \mathbf{R} \le 800$ $0.05 \le f \le 20$	**BCA10d** (Boore, et al. 2010)
$R \le 50$, $(R) = R^{-1}$; $R > 50$, $(R) = 50^{-1} * (\frac{R}{50})^{-0.5}$	$R = R_{hyp}$	$Q(f) = 410f^{0.5}$	$4.4 \le \mathbf{M} \le 5.0$ $23 \le \mathbf{R} \le 602$ $0.2 \le f \le 20$	**BS11** (Boatwright & Seekins, 2011)
$R \le 50$, $(R) = 10^{T_C C_{LF}} R^{-1.3}$; $R > 50$, $(R) = 50^{-1.3} * (\frac{R}{50})^{-0.5}$ f $\le 1, T_C = 1$; $1 < f < 5, T_C = 1 - 1.429 \log(f)$; $f \ge 5, T_C = 0$. $R \le h, C_{LF} = 0.2 \cos((\pi/2)(R-h)/(1-h))$; $10 < R < 50, C_L = 0.2 \cos((\pi/2)(R-h)/(1-h))$;	$R = (R_{hyp}{}^2 + h_{FF}{}^2)^{0.5}$, $h_{FF} = 10^{-0.405+0.235M}$ h = focal depth	$Q(f) = 525f^{0.45}$	$3.5 \le \mathbf{M} \le 6.0$ $10 \le \mathbf{R} \le 500$ $0.2 \le f \le 20$	**AB14** (Atkinson & Boore, 2014)

2.3 Upper-crust modification factors

The study of upper-crust modification effects, on ground motions, is a key topic in engineering seismology.

The upper-crust modification effect is modelled in two separate parts: amplification ($Am(f)$ in Eq. (1)) and attenuation ($An(f)$ in Eq.(1)) (same as diminishing) effects. The amplification effect is caused by the difference between the geological conditions of the two mediums that the shear wave is propagating. The attenuation effect is used to model the path-independent energy loss of the seismic wave (the path-dependent part is modelled by an anelastic attenuation factor).

The amplification factor is expressed as Eq. (14):

$$Am\ (f) = \sqrt{\frac{\rho_0 \beta_0}{\bar{\rho}_z \bar{\beta}_z}} \tag{14}$$

where ρ_0 and β_0 are the density and shear-wave velocity in the vicinity of the source; $\bar{\rho}_z$ and $\bar{\beta}_z$ are the time-averaged density and SWV over a depth corresponding to a quarter wavelength. In this study, the units of ρ_0 and β_0 are g/cm^3 and km/s respectively.

$\bar{\rho}_z$ and $\bar{\beta}_z$ can be computed from Eqs. (15a) and (15b) respectively.

$$\bar{\rho}_Z = \left(\int_0^{Z(f)} \rho(Z)dZ\right)/Z\ (f) \tag{15a}$$

$$\bar{\beta}_Z = Z\ (f)/\left(\int_0^{Z(f)} \frac{1}{\beta(Z)}\, dZ\right) \tag{15b}$$

In Eq. (15), $\rho(Z)$ and $\beta(Z)$ is the density and SWV at the depth of "Z" (near the surface). "Z" is defined as the "quarter wave-length" and this method of approximation is called as "Quarter Wavelength Approximation (QWA)" method (Boore, 2003), which is shown in Eq. (16):

$$Z = \frac{1}{4}\bar{\beta}/f \tag{16}$$

Combining Eq. (15) and (16), the implicit function of Z(f) and be expressed as Eq. (17):

$$f(Z) = 1/\left[4 \int_0^{Z(f)} \frac{1}{\beta(Z)}\, dZ\right] \tag{17}$$

The upper-crustal amplification factor calculated by Eq. (14) has been proved to be consistent with the wave propagation observations (Boore, 2003; Chen, 2000).

Eq. (14) indicates that the SWV profile ($\beta(Z)$) is of significant importance for modelling the site amplification factor.

Two different upper-crust amplification models (mainly for the shear-wave velocity profile model) are adopted in GMSS2.0. The first model is based on the reference generic rock site conditions for generally broad use (which is not proposed for any site-specific conditions) (Boore & Joyner, 1997; Boore, 2016). The second model is proposed for use in site-specific

conditions and to consider the intra-regional variance of the upper crust (Tang, Xiang, et al., 2020).

2.3.1 Reference generic rock site SWV profiling model for use in broad regions

The reference rock site method is widely used in developing modern GMPEs (Atkinson & Boore, 2014; Atkinson, 2004; Atkinson & Boore, 2006; Yenier & Atkinson, 2015; Allen, 2012). Usually, a specific value of V_{S30} (the time-averaged SWV at the top 30 m of soil sediment) is determined for a broad target region and the geological settings within the target region are assumed to be identical. Boore and Joyner (1997) (abbreviated as BJ97 model in the following context) constructed a SWV profiling model as a function of depth for generic rock (GR) site and generic very hard rock (GHR) site, based on borehole data and studies of upper-crustal SWV. Besides, Boore (2016) (abbreviated as the B16 model in the following context) put forward a simplified slowness (reciprocal of SWV) interpolation method to construct the SWV profile ($\beta(Z)$) with specific V_{S30} values using the profiles of GR site (V_{S30} = 0.62 km/s) and GHR site (V_{S30} = 2.78 km/s). The profiling models of the GR site and GHR site are summarized in Table 2 and Table 3 respectively.

Table 2. Generic Rock

Depth (km)	**SWV (km/s)**
$Z \leq 0.001$	0.245
$0.001 < Z \leq 0.03$	$2.206Z^{0.272}$
$0.03 < Z \leq 0.19$	$3.5426Z^{0.407}$
$0.19 < Z \leq 4.0$	$2.505Z^{0.199}$
$4.0 < Z \leq 8.00$	$2.927Z^{0.086}$

Table 3. Generic Hard Rock

Depth (km)	**SWV (km/s)**
0.0	2.768
0.05	2.808
0.1	2.847
0.2	2.922
0.5	3.122
0.75	3.260
$0.75 < Z \leq 2.2$	$3.324Z^{0.067}$
$2.2< Z \leq 8.0$	$3.447Z^{0.0209}$

The slowness interpolation method proposed by Boore (2016) can be summarized by the following functions from Eqs. (18) to (20).

The relation between slowness and SWV can be shown by Eq. (18):

$$S(Z) = \frac{1}{\beta(Z)} \tag{18}$$

Then a third slowness profile (which is the target profile waiting to be determined) can be derived from the linear interpolation of two generic slowness models (GR and GHR) by Eq. (19):

$$S(Z) = (1 - \varepsilon)S_1(Z) + \varepsilon S_2(Z) \tag{19}$$

where $S_1(Z)$ is the slowness of the GR site, and $S_2(Z)$ is the slowness of the GHR site at depth of Z km.

The weight coefficient ε can be determined by setting the average slowness equal to the desired value $\bar{S}_D$, and the value of ε can be determined by Eq. (20).

$$\varepsilon = \frac{\bar{S}_D - \bar{S}_1}{\bar{S}_2 - \bar{S}_1} \quad (20)$$

where $\bar{S}_1$ and $\bar{S}_2$ are the average slowness of GR and GHR over top 30 m respectively.

2.3.2 SWV profiling model considering intra-regional variances for site-specific use

Modern Probabilistic Seismic Hazard Analysis (PSHA) needs a higher requirement to deal with the intra-regional variance of upper-crust modification effects. To meet this requirement, Chandler et al. (2005) proposed a generic SWV profiling model which incorporates local geological information to minimize the intra-regional variance. This model is updated by Tang (2019) and validated using field SWV measurements collected from the CRUST1.0 database as well as various target subregions (e.g. Melbourne Region and Hong Kong Region). The detailed case-by-case SWV profiling model is summarized in Table 4.

Table 4. Partially non-ergodic SWV profiling model (Tang, 2019; Tang, Xiang, et al. 2020)

Case	Depth range (km)	β (km/s)
Case 1 ($Z_S \geq 2$)	$0 < Z \leq 0.2$	$\beta_{0.03}\,(Z/0.03)^{0.3297}$
	$0.2 < Z \leq 2$	$\beta_{0.2}\,(Z/0.2)^{0.1732}$
	$2 < Z \leq Z_S$	$\beta_2\,(Z/2)^{0.1667}$
	$Z_S < Z \leq Z_C$	$\beta_{ZC}\,(Z/Z_C)^n$
	$Z_C < Z$	$\beta_8\,(Z/8)^{0.0833}$
Case 2 ($0.2 < Z_S < 2 \leq Z_C$)	$Z \leq 0.2$	$\beta_{0.03}\,(Z/0.03)^{0.3297}$
	$0.2 < Z \leq Z_S$	$\beta_{0.2}\,(Z/0.2)^{0.1732}$
	$Z_S < Z \leq Z_C$	$\beta_{ZC}\,(Z/Z_C)^n$
	$Z_C < Z$	$\beta_8\,(Z/8)^{0.0833}$
Case 3 ($0.2 < Z_S < Z_C \leq 2$)	$0 < Z \leq 0.2$	$\beta_{0.03}\,(Z/0.03)^{0.3297}$
	$0.2 < Z \leq Z_S$	$\beta_{0.2}\,(Z/0.2)^{0.1732}$
	$Z_S < Z \leq Z_C$	$\beta_{ZC}\,(Z/Z_C)^n$
	$Z_C < Z \leq 2$	$\beta_2\,(Z/2)^{0.0899}$
	$2 < Z$	$\beta_8\,(Z/8)^{0.0833}$
Case 4 ($Z_S < 0.2 < 2 \leq Z_C$)	$0 < Z \leq Z_S$	$\beta_{ZI}\,(Z/Z_I)^{0.3297}$
	$Z_S < Z \leq Z_C$	$\beta_{ZC}\,(Z/Z_C)^n$
	$Z_C < Z$	$\beta_8\,(Z/8)^{0.0833}$
Case 5 ($Z_S < 0.2 < Z_C \leq 2$)	$Z \leq Z_S$	$\beta_{ZI}\,(Z/Z_I)^{0.3297}$
	$Z_S < Z \leq Z_C$	$\beta_{ZC}\,(Z/Z_C)^n$
	$Z_C < Z \leq 2$	$\beta_2\,(Z/2)^{0.0899}$
	$2 < Z$	$\beta_8\,(Z/8)^{0.0833}$
Case 6 ($Z_C \leq 0.2$)	$0 < Z \leq Z_S$	$\beta_{ZI}\,(Z/Z_I)^{0.3297}$
	$Z_S < Z \leq Z_C$	$\beta_{ZC}\,(Z/Z_C)^n$
	$Z_C < Z \leq 0.2$	$\beta_{0.2}\,(Z/0.2)^{0.2463}$
	$0.2 < Z \leq 2$	$\beta_2\,(Z/2)^{0.0899}$
	$2 < Z$	$\beta_8\,(Z/8)^{0.0833}$

(Z_S and Z_C are the thickness of the upper sediment layer and total sediment layers respectively; $\beta_{0.03}$, $\beta_{0.2}$, β_2 and β_8 are the SWV value at the depth of 0.03, 0.2, 2, and 8 km; β_{ZS} and β_{ZC} are the V_S value at the depth of Z_S and Z_C respectively. $Z_I = \min(Z_S, 0.03)$)

In GMSS2.0, the density profile is adopted from the study performed by Brocher (2005). The SWV profiles constructed by the BJ model (GR and GHR site) and by Tang (2019) (for

Melbourne Region and Hong Kong Region) up to 50 km are shown in Fig. 3 (a), and the corresponding frequency-dependent amplification up to 100 Hz are shown in Fig. 3 (b).

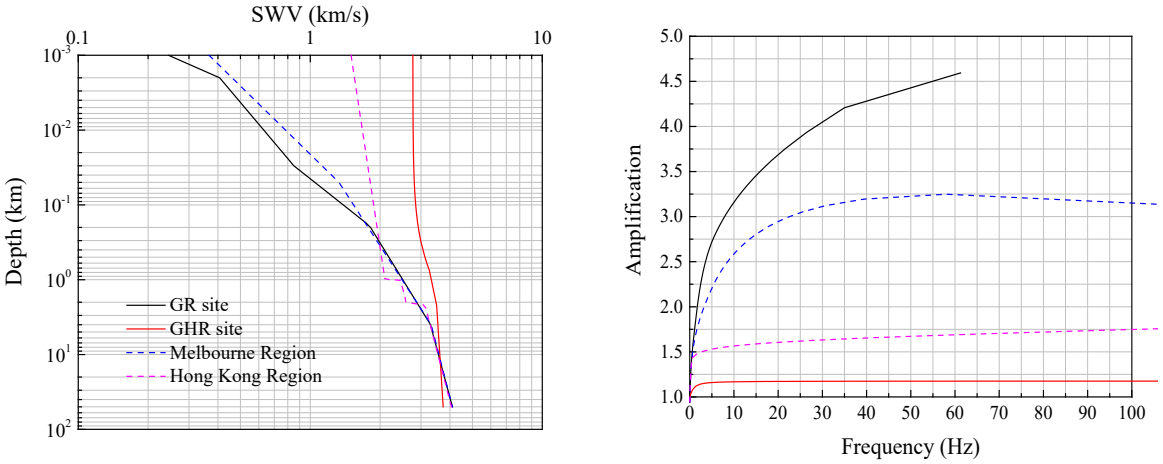

(a) SWV profiles (b) Frequency-dependent amplitude

Figure 3. SWV profiles constructed by the BJ model (solid lines) and Tang (2019) model (dash lines), and the corresponding frequency-dependent amplitude factors.

Another method to define the site effects is to obtain the frequency-dependent amplification factor empirically (Atkinson and Boore, 2006).

The last important factor is the upper-crust attenuation factor. The attenuation factor can be represented by two different forms, shown by Eqs. (21) and (22) respectively.

$$An(f) = [1 + (f/f_{max})^8]^{-1/2} \tag{21}$$

$$An(f) = exp\,(-\pi\kappa_0 f) \tag{22}$$

In this study, both Eqs. (21) and (22) are adopted in the GMSS and users can choose either one based on their preferences.

3. Principles of GMSS2.0

GMSS2.0 is a software package used for generating synthetic accelerograms based on stochastic simulations of seismological models. The particular feature of GMSS2.0 is that all the procedures can be run transparently and any user can use it without a solid background in seismology. The general procedures of GMSS2.0 are illustrated in Fig. 4. The detailed principle of GMSS2.0 is introduced step by step in this section.

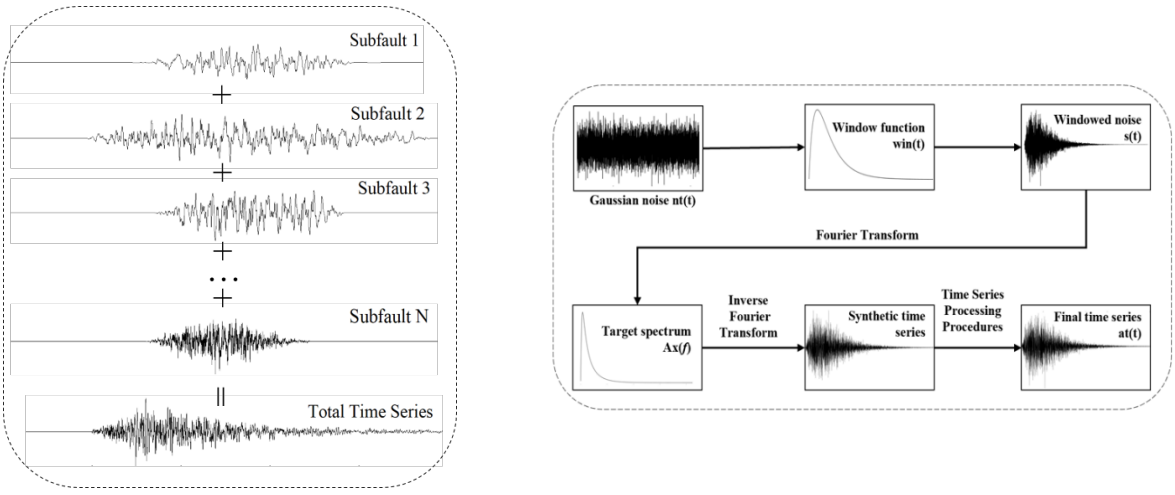

(a) Overall finite-fault simulation (b) Single subfault simulation

Figure 4. General procedures of synthetic accelerograms generation in GMSS2.0 (Tang, 2022(b))

The detailed implementation procedures of GMSS2.0 are given in the following sections.

3.1 Generation of Gaussian white noise and filter for a single subfault

Gaussian white noise is used for mimicking the random phenomenon of the seismic waves radiated from the source. Gaussian white noise can be generated by a random number generator that has been built into the computer and can be accessed from many platforms including MATLAB. The white noise must be band-limited in between the lowest frequency value "df" (which is reciprocal of the total duration of the simulated time-history) and the highest frequency (N/2-1) df (Nyquist frequency) where N is the number of time-steps in the simulation.

A 4-level acausal Butterworth filter with a "bandpass" form is adopted in this study. This specific filter is adopted because it is also used in the establishing process of the PEER NGA-East Database (Goulet, et al. 2014). Additionally, according to Boore and Akkar (2003), the acausal filter is preferred for the calculation of response spectra, because the results are not dependent on the selected filter frequency.

A typical band-limited Gaussian noise is shown in Fig. 5.

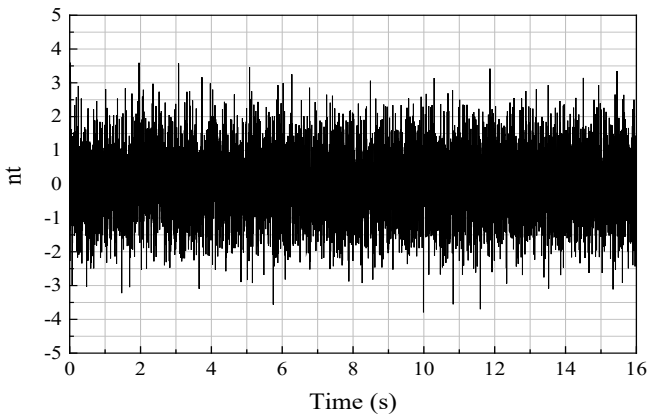

Figure 5. An example of band-limited Gaussian noise

3.2 Window function

A window function win(t) is then applied to modulate the signal in the time domain (as shown in Fig. 5).

Essentially,

$$st(t) = win(t) \times nt(t) \tag{23}$$

where *nt(t)* are the band-limited Gaussian noise before the imposition of windowing; *win(t)* is the imposed time window function that has been scaled in such a way not to alter the overall amplitude of the Gaussian noise. The windowing function *win(t)* can be of the trapezoidal or exponential form (the window form does not draw many influences on response spectra). The latter has been adopted in this study and is defined by Eq. (24) (Lam et al., 2000):

$$win(t) = e^{-0.4t(6/T_d)} - e^{-1.2t(6/T_d)} \tag{24}$$

In the study of Boore (2003), the window function is defined as Eq. (25):

$$win(t) = 26.312(t/2T_d)^{1.253} e^{-6.266(t/2T_d)} \tag{25}$$

Both in Eqs. (24) and (25),

$$T_d = T_0 + T_p \tag{26a}$$

$$T_0 = r/2V_{rup} \tag{26b}$$

$$T_p = bR \tag{26c}$$

where T_d is the total ground motion duration, and T_0 is source duration, T_p is path duration (as mentioned in Section 2.2). r is the fault radius in km, V_{rup} is the rupture velocity in km/s, R is the distance, and b is a distance-dependent coefficient. The distance-dependent duration (path duration) is an important factor as well because the peak ground motions will decrease with distance increases. Empirical observations and theoretical simulations suggest that path duration can be modelled by several connected straight-line segments (Boore, 2003). In this study, *b* would be fixed at 0.05 at all distances for simplicity if no further information is given.

In GMSS2.0, users can define the path duration for real situations by inputting the self-defined input file.

The window functions win(t) described by Eqs. (24) and (25) are shown in Fig. 6, in which T_d is assumed to be 10 s for both functions.

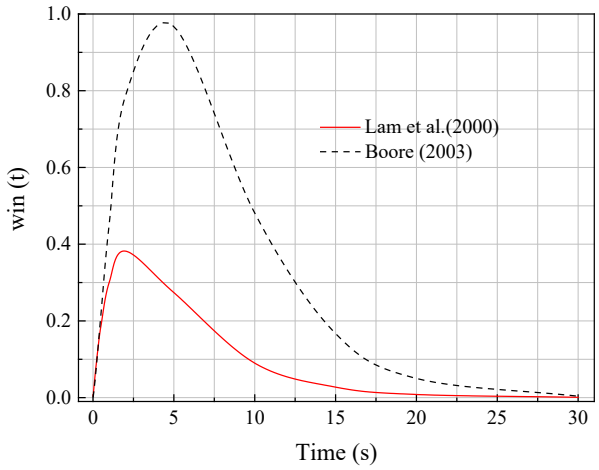

Figure 6. Window function *win(t)*, T_d = 10 s for both functions

st(t) in Eq. (22) is the windowed noise and there is an ensemble of such noise time series with random variability within them. An example of *st(t)* is illustrated in Fig. 7, for a single subfault.

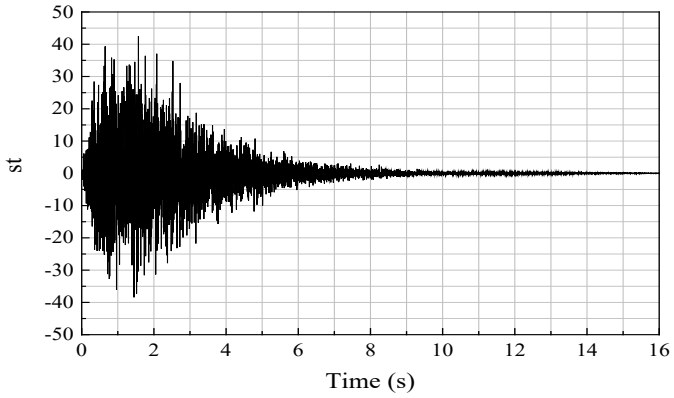

Figure 7. An example of windowed noise st(t)

3.3 Fourier Transform of windowed noise

The purpose of the Fourier transform is to find the Fourier amplitudes of the windowed noises, which have random variability within different simulations and are averaged to unity across the simulated accelerogram ensembles. The set of phase angles obtained from the Fourier transform is reserved for use in the inverse Fourier transform procedure to remove any possible uncertainties introduced in the two procedures (fast Fourier transform and inverse Fourier transform). The basic expressions of the "*fft*" function in MATLAB and the inverse process can be expressed as Eqs. (27a) and (27b).

$$X(k) = \sum_{r=1}^{N} x(r) exp\ (-j2\pi(k-1)(r-1)/N) \quad (27a)$$

$$x(r) = (1/N) \sum_{k=1}^{N} X(k) exp\ (j2\pi(k-1)(r-1)/N) \quad (27b)$$

where $X(k)$ is the Fourier amplitude signal and $x(r)$ is the original signal, N is the total number of the time step.

After the Fourier transform, the spectrum of the noise is noted as *As(f)*. An example spectrum is shown in Fig. 8, for a single subfault.

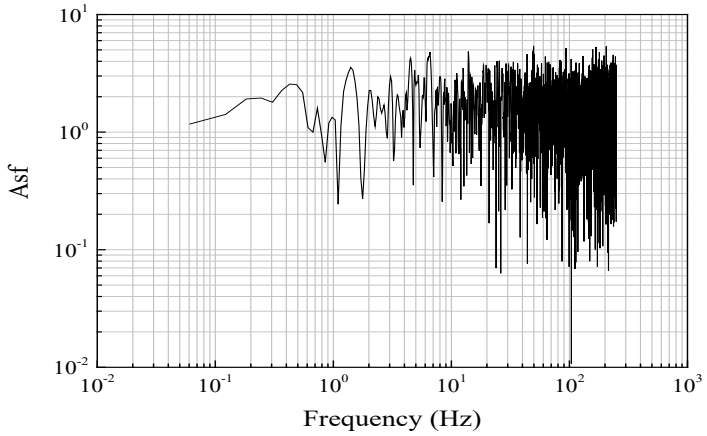

Figure 8. An example of a noise signal after Fourier Transform *As(f)*

3.4 Target spectrum and filtered spectrum

The seismological model identified in Section 2 is the frequency filter *Ax*(*f*) which defines the frequency content of the ground motion in the form of a Target Fourier Amplitude Spectrum as illustrated in Fig. 9. A summary of the well-publicized, and established, seismological models (including source models, attenuation functions, and upper-crust modification factors) has been presented in Section 2. A more detailed introduction to the concept of seismological modelling can be found in the study performed by Boore (2003).

Next step is filtering windowed noise signal (*As*(*f*)) by the seismological model *Ax*(*f*) - Fourier Amplitude Spectrum. *Aa*(*f*) is essentially a product of *As*(*f*) and Ax(*f*). Aa(*f*) obtained from an individual simulation may contain considerable random variabilities. Importantly, the ensemble-averaged *Aa*(*f*) as derived from repetitive simulations should display convergence to Ax(*f*). An example of Target spectrum ($\Delta\sigma$ = 200 bar**,** M = 6, R = 30 km, Q_0 = 680, n = 0.36, no upper-crust modification effect), *Ax*(*f*), and the filtered spectrum *Aa*(*f*) are shown in Fig. 10.

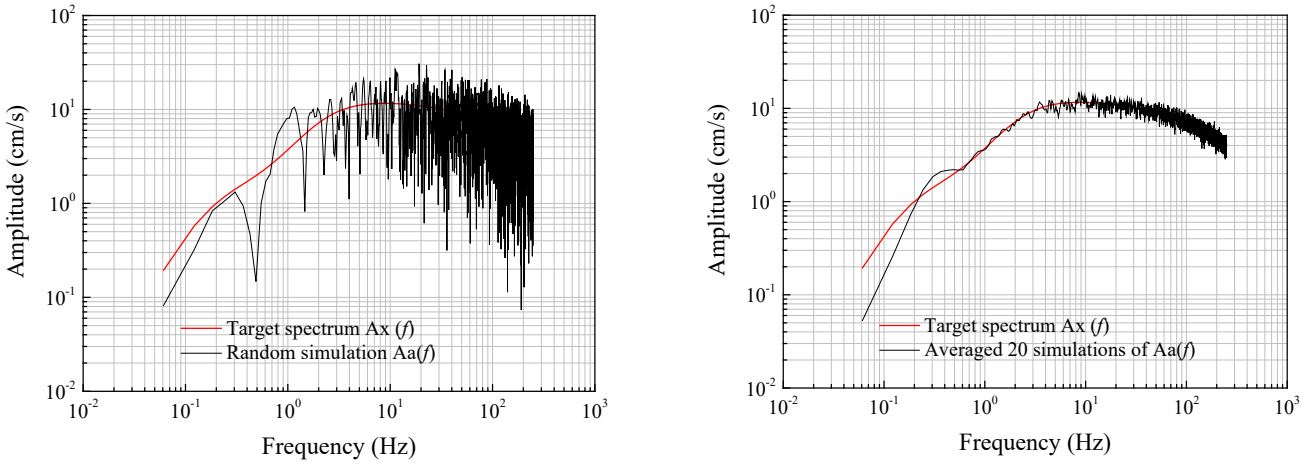

(a) One random simulation

(b) average of 10 random simulations

Figure 9. An example of the target spectrum and random simulations

It is important to perform the procedures stated above in the order strictly, otherwise, some unexpected results would be obtained. For example, if the noise *nt(t)* is filtered by a seismological model *Ax*(*f*) first and then windowed by window function *win(t)*, the long-period level of the motion will be distorted, and this result is also reported in Boore (2003).

3.5 Generation of time series and time series processing procedures

The next step is the inverse Fourier Transform of the windowed-filtered noise signal – Inverse Fourier Transform of *Aa*(*f*) whilst incorporating the phase angles obtained from Fourier Transform to give the ground motion time-series *a(t)*. This procedure is straightforward. However, the time series obtained from the procedures stated above cannot be used for engineering applications directly.

Till now the time series for a single subfault has been completed. The next step is to sum all the time series of each subfault to get the final time series for the whole fault source. The time delay of each subfault is calculated from the path delay and the random source delay (shown in Eq. 12).

Further time series processing procedures are required to obtain a more reliable time series.

According to Boore (2005), response spectra and peak ground motions should be computed from the complete, padded time series, not from the pad-stripped data directly. Pad-stripped time series which are provided by data agencies can be misleading for computing peak ground motions or response spectra. The ground-motion intensity measures such as peak velocity and response spectral amplitudes provided by the agencies which are obtained from the complete padded and filtered acceleration time series may be different from the computed results based on the pad-stripped time series. This also implies that using the pad-stripped time series for any analysis, such as the response of a nonlinear structure, is inconsistent use of the time series

(Boore, 2009b). The time series of recorded data in the NGA database are always pad-stripped data. One reason for only providing pad-stripped time series might be because plots of the padded and filtered accelerations would appear to have a long section of zero motion before the arrival of the shaking, and users might be tempted to remove this section of the time series. Doing so, however, may lead to distortions in quantities such as peak displacements and oscillator response derived from the truncated time series (Boore, et al. 2012). The time series of accelerograms generated by an original program like GENQKE and SMSIM (the version before 2002) is just like the pad-stripped data in the database.

Baseline correction, or zeroth-order correction, is also required which should be combined with the filter, to help to obtain the correct simulations. GMSS2.0 provides 5 different choices for end-users to perform baseline correction, which are listed in Table 5. Moreover, pre-event and after-event time pads are required to add to the time series to ensure the displacement time series will not distort at long durations (especially required for filtering approaches).

For calculating the time series of velocity and displacement, the general approach is numerical integration. The Northbridge integration method is adopted for this purpose. Refer to Fig. 10 for a typical sample of the simulated time series which are presented in the form of the acceleration, velocity, and displacement formats, for before and after TSPP.

Table 5. Baseline correction methods used in GMSS2.0

No.	Method	Basic principle	Type	Reference
1	G79	Use a polynomial to mimic the trend in the velocity trace and subtract the derivative of the polynomial in the original acceleration trace	Empirical piecewise	(Graizer, 1979)
2	C97	Use a polynomial to mimic the trend in the original acceleration trace and apply the band-pass filter to the trace additionally	Filtering	(Chiu, 1997)
3	B05	Apply the low-cut filter to the acceleration in the Fourier domain	Filtering	(Boore, 2005)
4	J10	Use a polynomial to mimic the trend in the velocity trace and subtract the derivative of the polynomial in the original acceleration trace	Empirical piecewise	(Jiang, 2010)
5	P18	Use a polynomial to mimic the trend in the velocity trace and subtract the derivative of the polynomial in the original acceleration trace	Empirical piecewise	(Papazfeiropoulos and Plevis, 2018)

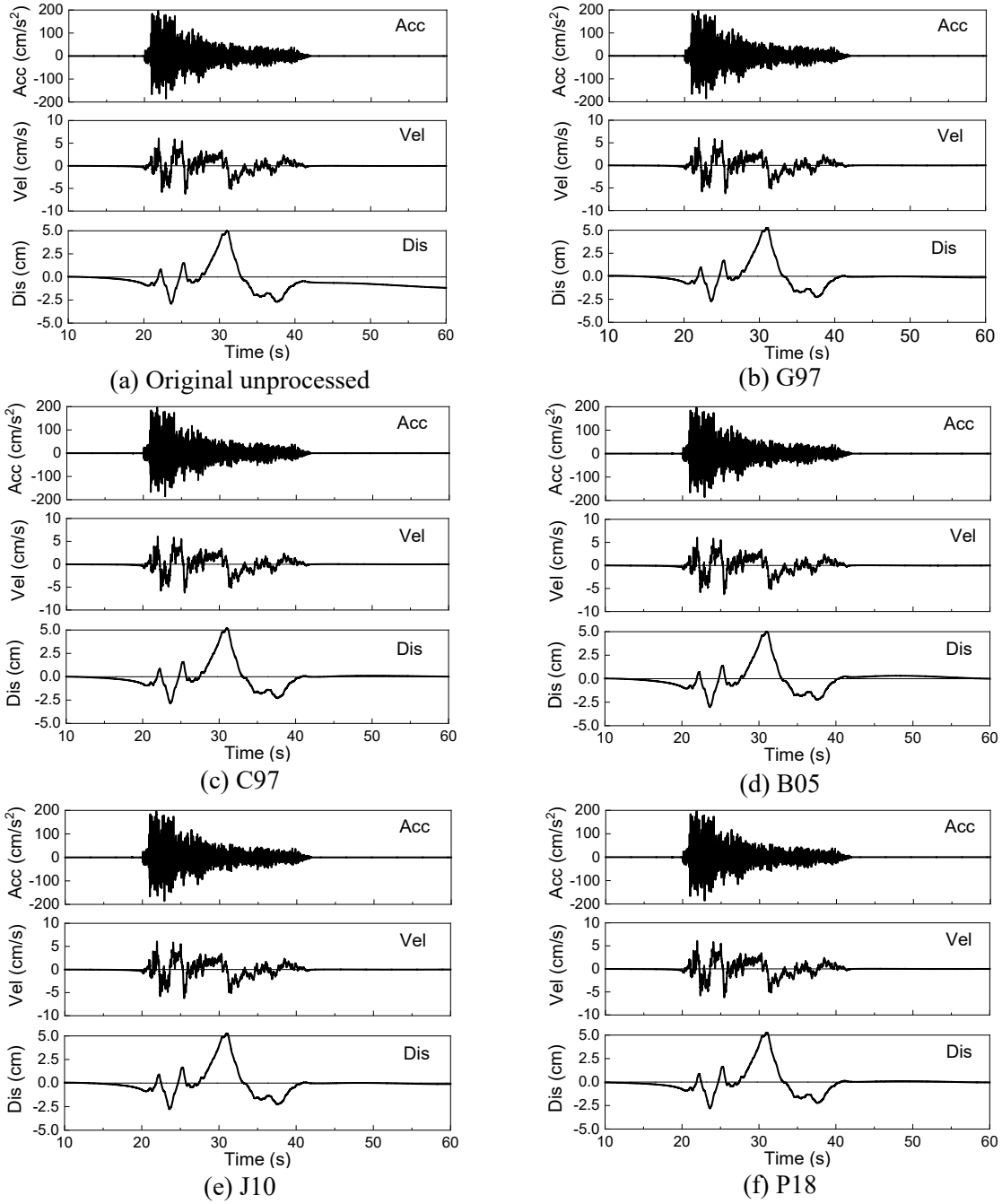

Figure 10. Simulated ground motion time series, before and after Time Series Processing Procedures (TSPP).

3.6 Computation of response spectra

By definition, the response spectrum (it can be acceleration, velocity, or displacement) describes the maximum response of a single-degree-of-freedom (SDOF) oscillator to a specific input ground motion. Response spectrum does not describe real ground motion, and it only provides information on how SDOF oscillators respond to the input ground motion. Structures are usually approximated by SDOF oscillators in engineering practice and structures with different heights correspond to the oscillators with different natural circular frequencies (F_n) or natural periods (T_n). Response spectrum is a function of the natural circular frequency and

damping ratio (ξ) of a suite of SDOF oscillators. In practice, the damping ratio (ξ) is assumed to be the same for all oscillators (Robinson, et al. 2006).

Analytical solution of the equation of motion for a SDOF system is usually not possible if the excitation (applied force or ground acceleration) varies arbitrarily with time or if the system is nonlinear. Such problems can be tackled by numerical time-stepping methods for the integration of differential equations (Chopra, 2 007). The time-stepping method, namely the Central Difference Method (CFD), will be adopted to construct the response spectrum in this study. Detailed mathematic expressions can be found from Eqs. (29) to (33).

Getting started from the dynamic equation of a simple SDOF system:

$$m\ddot{u} + c\dot{u} + ku = p(t) \tag{29}$$

If the time step integration method is adopted, Eq. (28) can be expressed as Eq. (30):

$$m\ddot{u}_i + c\dot{u}_i + ku_i = p(t_i) \tag{30}$$

Eq. (30) can be obtained by dividing the mass from both sides of Eq. (31):

$$\ddot{u}_i + 2\xi\omega_n\dot{u}_i + \omega_n^2 u_i = -\ddot{u}_{gi} \tag{31}$$

Eq. (31) can be obtained from the definition of "slope":

$$\dot{u}_i = \frac{u_{i+1}-u_{i-1}}{2\Delta t} \tag{32a}$$

Similarly,

$$\ddot{u}_i = \frac{u_{i+1}-2u_i+u_{i-1}}{\Delta t^2} \tag{32b}$$

Finally, Eq. (33) can be obtained by combining Eqs. (31) and (32):

$$u_{i+1} = \frac{-\ddot{u}_{gi}+\left(\frac{2}{\Delta t^2}-\omega_n^2\right)u_i+\left(\frac{\xi\omega_n}{\Delta t}-\frac{1}{\Delta t^2}\right)u_{i-1}}{\frac{1}{\Delta t^2}+\frac{\xi\omega_n}{\Delta t}} \tag{33}$$

This is the foundation of the calculation of displacement response spectrum, and using the relationship between displacement and velocity, acceleration, all response spectra can be computed. The detailed meaning of each parameter is shown in Eqs. (29 - 33) is given in Table 5.

Table 6. Parameters used in the Central Difference Method

Parameter	Meaning	Unit
m	Structure mass	kg
c	Viscous damping	/
k	Structure stiffness	/
$\ddot{u}$	Ground motion acceleration	m/s^2
$\dot{u}$	Ground motion velocity	m/s
u	Ground motion displacement	m
$p(t)$	External excitation	N
ξ	Damping ratio (as a proportion of critical damping value)	/
ω_n	Angular velocity	rad/s
Δt	Time interval	s

4. Subroutine Functions in GMSS2.0

4.1 Fault size

I the exact dimension of the target fault is not available, empirical scaling laws can be employed to compute the fault sizes. Accurate estimates of fault sizes are important to determine the site-rupture distances. GMSS2.0 provides 4 different scaling laws to compute the fault size, and end-users may choose the most suitable one to use. Detailed information is listed in Table 7 (Tang, 2022b).

Table 7. Rupture scaling relationships used in GMSS2.0

Relationship	**WC94** (Wells and Coppersmith, 1994)	**L10** (Leonard, 2010)	**K17** (Kumar, et al. 2017)	**C19** (Cheng, et al. 2019)
Normal	$FL = 10^{-1.88+0.50M}$ $FW = 10^{-1.14+0.35M}$	$FL = 10^{-2.54+0.60M}$ $FW = 10^{-1.46+0.40M}$	$FL = 10^{-1.722+0.485M}$ $FW = 10^{-0.829+0.323M}$	$FL = 10^{-4.02+0.83M}$ $FW = 10^{-2.13+0.51M}$
Reverse	$FL = 10^{-2.42+0.58M}$ $FW = 10^{-1.61+0.41M}$	$FL = 10^{-2.54+0.60M}$ $FW = 10^{-1.46+0.40M}$	$FL = 10^{-2.693+0.614M}$ $FW = 10^{-1.669+0.435M}$	$FL = 10^{-3.27+0.72M}$ $FW = 10^{-1.67+0.44M}$
Strike-slip	$FL = 10^{-2.57+0.62M}$ $FW = 10^{-0.76+0.27M}$	$FL = 10^{-2.50+0.60M}$ $FW = 10^{-1.49+0.40M}$	$FL = 10^{-2.943+0.681M}$ $FW = 10^{-0.543+0.261M}$	$FL = 10^{-2.45+0.61M}$ $FW = 10^{-1.38+0.41M}$
Undefined	$FL = 10^{-2.44+0.59M}$ $FW = 10^{-1.01+0.32M}$	$^{*}FL = 10^{-2.59+0.60M}$ $^{*}FW = 10^{-1.60+0.40M}$	$^{\dagger}FL = 10^{-2.412+0.583M}$ $^{\dagger}FW = 10^{-0.88+0.366M}$	$FL = 10^{-2.67+0.63M}$ $FW = 10^{-1.38+0.40M}$

(Note: FL and FW is the fault length and width respectively; M is the moment magnitude; FW in L10 is obtained using the correlation between fault area and FL, assuming the fault is rectangular; FW in C19 is obtained using the correlation between FL and FW. The unit for FL and FW is km in this study; "*" means this scaling relationship is specifically for Stable Continental Region; "†" means this scaling relationship is specifically for Subduction Interface. C19 is typical for China mainland)

4.2 Site location

GMSS2.0 provides two opinions for localizing the site, and end-users can input the *longitude and latitude*, or the *reference distance and azimuth* (to the **reference point**, not epicentre), to find the location of the site. The function "*FUNSL*" is used for this purpose in GMSS2.0.

4.3 Site distances

GMSS2.0 provides 7 different types of distances for use in simulating ground motions. The basic definition of the distances is listed in Table 8.

Table 8. Distance types in GMSS2.0

No.	Symbol	Definition
1	R	Reference distance (equal to epicentral distance if the epicentre is the reference point)
2	R_{hyp}	Hypocentral distance
1	R_{rup}	Closest distance to the fault rupture
2	R_{jb}	Closest distance to the surface projection of the fault rupture
3	R_{seis}	Closest distance to the rupture portion in the seismogenic crust
4	R_x	Horizontal distance perpendicular to the rupture strike
5	R_{y0}	A distance along strike

To verify the distance functions, I compared the distance computed from GMSS2.0 and EXSIM_DMB for three different faults at 7 sites. The plan of the faults and sites is shown in Fig.11, and detailed information about the faults and sites are listed in Table 9 and Table 10 (this is adopted from daveboore.com).

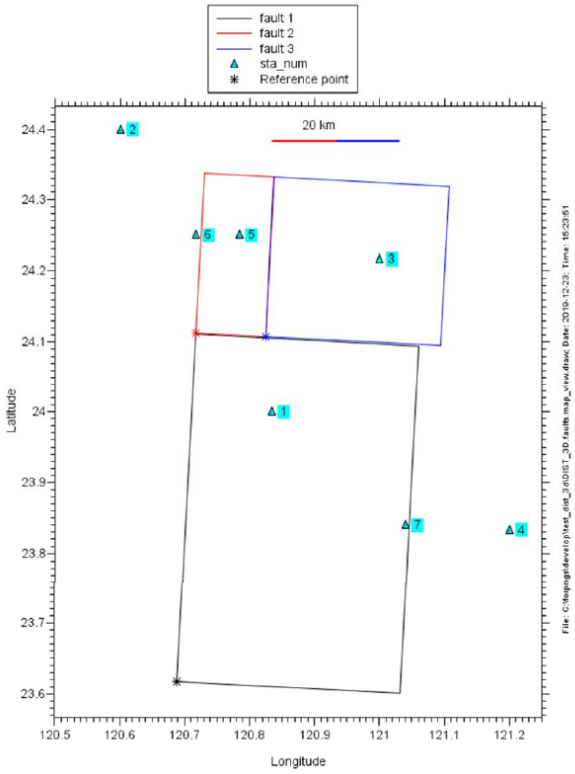

Figure 11. Fault and site plan

Table 9. Information of the faults

Fault	Lat	Lon	Strike	Dip	h	S1	S2	W1	W2
1	23.617	120.689	3	29	0.94	0	55	0	40
2	24.113	120.717	3	29	0.94	0	25	0	12.5
3	24.108	120.824	3	5	7	0	25	0	27.5

(Note: The latitude and longitude and the depth (h) are for the reference point (the red star point in Fig.11). S1 and S2 are the distance along strike near the edge and far edge; W1 and W2 are the distance down dip near the edge and far edge (for the reference point).

Table 10. Information of the sites

Site	Lat	Lon
1	24	120.8333
2	24.4	120.6
3	24.21666	121
4	23.83333	121.2
5	24.25	120.7833
6	24.25	120.7167
7	23.84	121.04

The comparison results for each fault are shown in Figs.12 - 14.

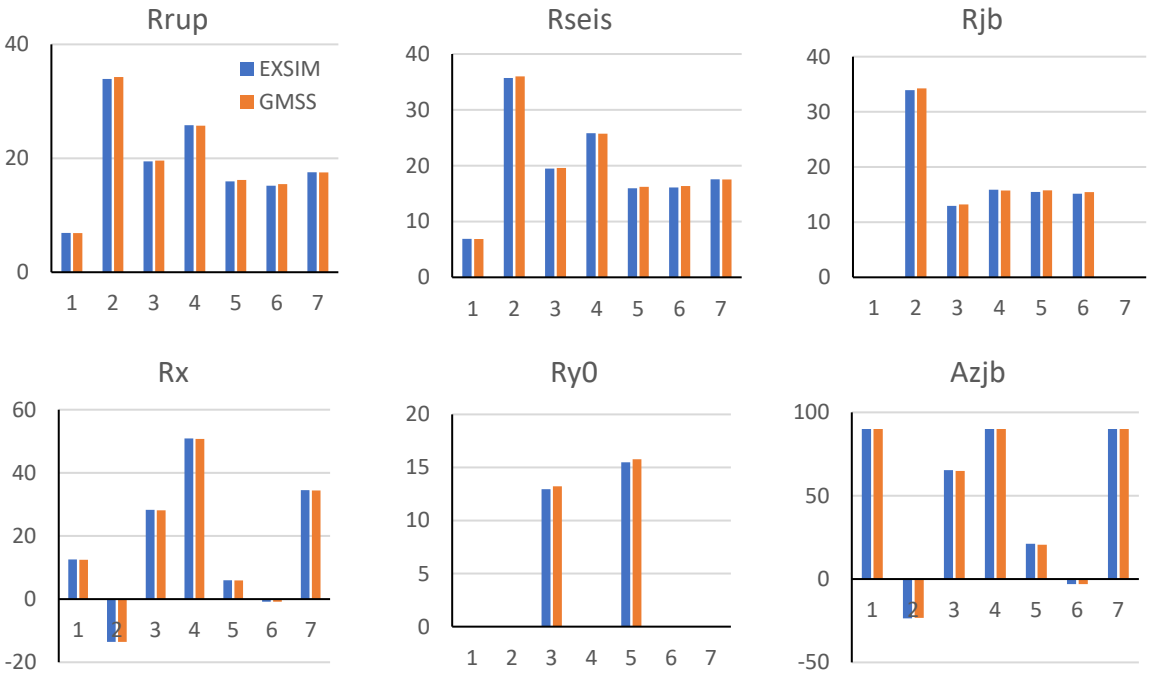

Figure 12. Fault 1

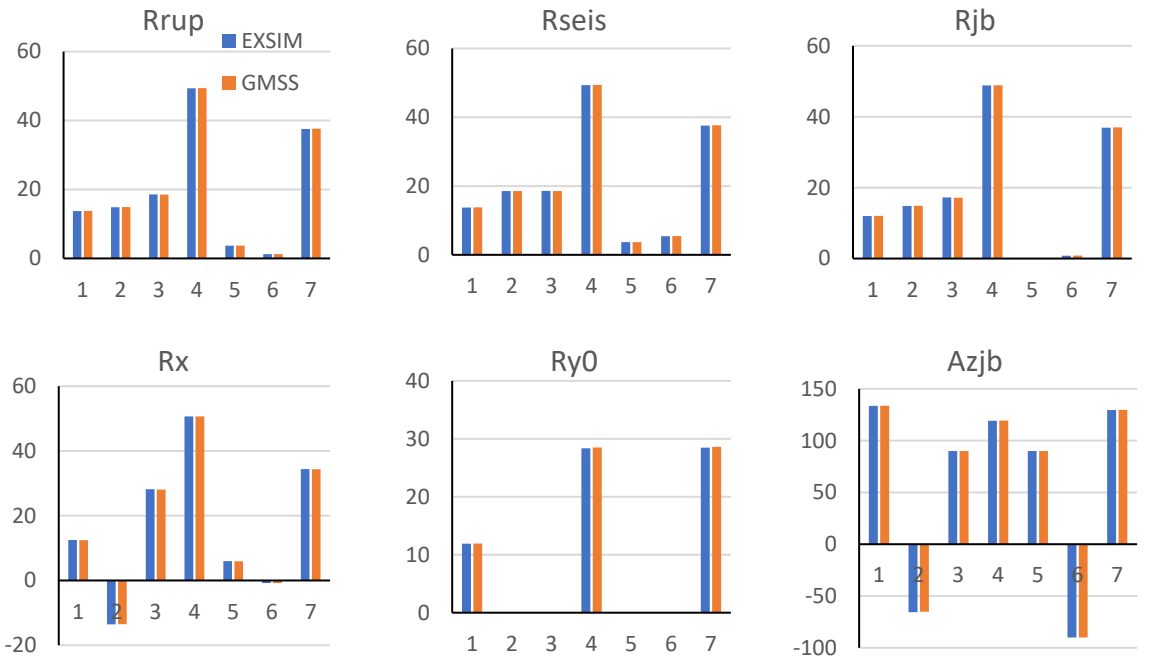

Figure 13. Fault 2

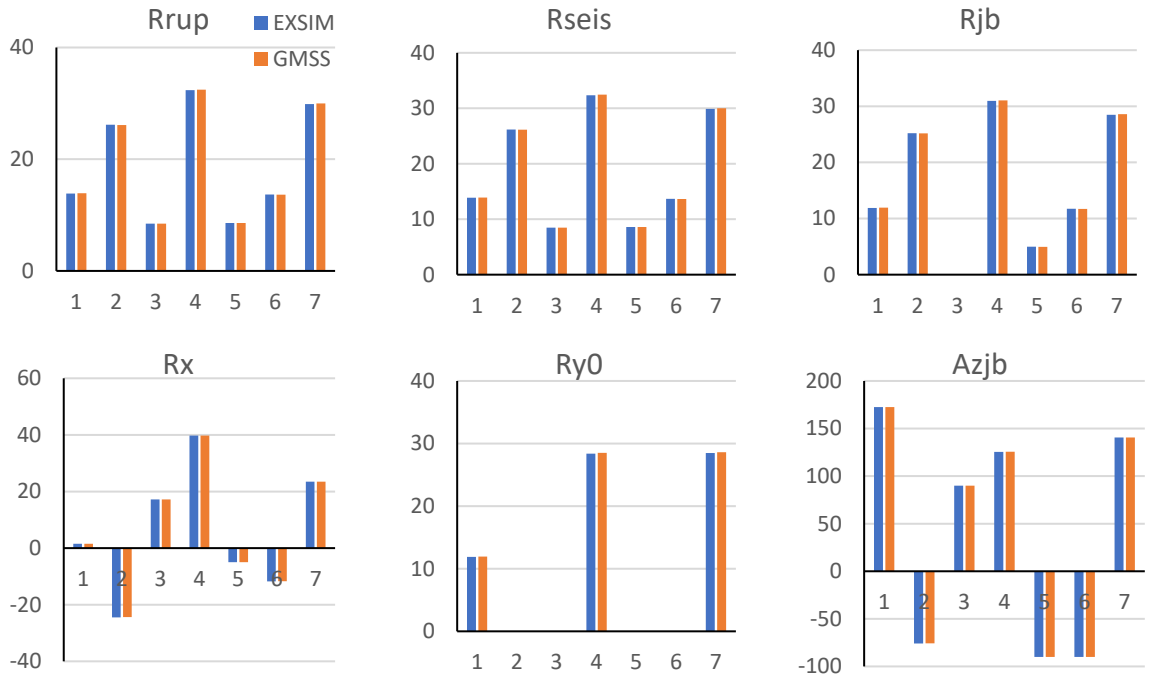

Figure 14. Fault 3

The function "*FUNDist*" is used for distances computation in GMSS2.0.

4.4 Average calculations

In GMSS2.0, the arithmetic average (mean) is taken over the number of simulations, and the geometric average (median) is taken over the number of random hypocentres. The function "*FUNCalAve*" is used for this purpose in GMSS2.0.

4.5 Notes for GMSS2MS

In GMSS2MS, which is for multiple scenario simulations, special attention should be paid to some points. First, the pre-determined time-step is required in this subroutine. If an error similar to "*Unable to perform assignment because the size of the left side is 1-by-16384 and the size of the right side is 1-by-32768*" shows up when running, this means the "NT" value needs to be adjusted. Second, the "Output. mat" file only contains the average value for simulated intensities (e.g. PGA) for each site, and this output can be modified according to the specific requirement by easy coding. Third, the subroutine functions that need custom change are listed separately in the folder "GMSS2.0-MS", other subroutine functions which cannot be changed are embodied in the main routine "GMSS2MS".

Acknowledgments

The guidance and encouragement from Dr. David Boore are deeply acknowledged.

References

Allen, T. I. (2012). Stochastic ground-motion prediction equations for southeastern Australian earthquakes using updated source and attenuation parameters. Canberra.

Atkinson, G., & Boore, D. (1995). Ground-Motion Relations for Eastern North America. Bulletin of the Seismological Society of America, 85, 17-30.

Atkinson, G. M. (2004). Empirical Attenuation of Ground Motion Spectral Amplitudes in Southeastern Canada and the Northeastern United States. Bull. Seismol. Soc. Am., 94, 1079-1095.

Atkinson, G. M., & Boore, D. M. (2006). Earthquake Ground-Motion Prediction Equations for Eastern North America. Bull. Seismol. Soc. Am., 96(6), 2181-2205.

Atkinson, G. M., & Boore, D. M. (2014). The attenuation of Fourier amplitudes for rock sites in eastern North America. Bull. Seism. Soc. Am, 104, 513-528.

Atkinson, G. M., & Boore, D. M. (2014). The Attenuation of Fourier Amplitudes for Rock Sites in Eastern North America. Bull. Seismol. Soc. Am., 104(1), 513-528.

Atkinson, G. M. and K. Assatourians (2015). Implementation and Validation of EXSIM (A Stochastic Finite-Fault Ground-Motion Simulation Algorithm) on the SCEC Broadband Platform, Seismol. Res. Lett. 86(1), 48-60.

Boatwright, J., & Seekins, L. (2011). Regional Spectral Analysis of Three Moderate Earthquakes in Northeastern North America. Bull. Seism. Soc. Am, 101, 1769-1782.

Baker, J.W. 2011. Conditional Mean Spectrum: Tool for Ground-Motion Selection, Journal of Structural Engineering, Vol 137(3) 322-331.

Baker, J.W. and Jayaram, N., (2008) "Correlation of spectral acceleration values from NGA ground motion models," Earthquake Spectra, 24(1), 299-317.

Boore, D. (1983). Stochastic simulation of high-frequency ground motions based on seismological models of the radiated spectra. Bull. Seism. Soc. Am, 73, 1865-1894.

Boore, D. M. (2003). Simulation of Ground Motion Using the Stochastic Method. Pure Appl. Geophys., 160, 635-676.

Boore, D. M. (2005). On Pads and Filters: Processing Strong-Motion Data. Bull. Seism. Soc. Am., 95(2), 745-750.

Boore, D. M. (2009a). Comparing Stochastic Point-Source and Finite-Source Ground-Motion Simulations: SMSIM and EXSIM. Bull. Seismol. Soc. Am., 99(6), 3202-3216.

Boore, D. (2009b) TSPP---A Collection of FORTRAN Programs for Processing and Manipulating Time Series. U.S. Geological Survey Open-File Report 2008-1111: USGS.

Boore, D. M. (2015). Point-Source Stochastic-Method Simulations of Ground Motions for the PEER NGA-East Project.

Boore, D. M. (2016). Short Note: Determining Generic Velocity and Density Models for Crustal Amplification Calculations, with an Update of the Boore and Joyner (1997) Generic Amplification for Vs(Z)=760 m/s. Bull. Seismol. Soc. Am., 106(1), 316-320.

Boore, D. M., & Akkar, S. (2003). Effect of causal and acausal filters on elastic and inelastic response spectra. Earthquake Engng Struct. Dyn., 32, 1729-1748.

Boore, D., Sisi, A. A., & Akkar, S. (2012). Using Pad-Stripped Acausally Filtered Strong-Motion Data. Bulletin of the Seismological Society of America, 102, 751-760.

Boore, D. M., Alessandro, C. D., & Abrahamson, N. A. (2014). A Generalization of the Double-Corner-Frequency Source Spectral Model and Its Use in the SCEC BBP Validation Exercise. Bull. Seismol. Soc. Am., 104(5), 2387-2398.

Boore, D. M., Campbell, K. W., & Atkinson, G. M. (2010). Determination of stress parameter for eight well-recorded earthquakes in eastern North America. Bull. Seismol. Soc. Am., 100, 1632-1645.

Boore, D. M., & Joyner, W. B. (1991). Estimation of Ground Motion at Deep-Soil in Eastern North America. Bull. Seism. Soc. Am., 81(6), 2167-2185.

Boore, D. M., & Joyner, W. B. (1997). Site Amplifications for Generic Rock Sites. Bull. Seismol. Soc. Am., 87(2), 327-341.

Brocher, T. M. (2005). Empirical Relations between Elastic Wavespeeds and Density in the Earth's Crust. Bull. Seismol. Soc. Am., 95(6), 2081-2092.

Brune, J. N. (1970). Tectonic stress and the spectra of seismic shear waves from earthquakes. J. Geophys.Res, 75, 4997-5009.

Chandler, A. M., Lam, N. T. K., & Tsang, H. H. (2005). Shear wave velocity modelling in crustal rock for seismic hazard analysis. Soil Dynamics and Earthquake Engineering, 25, 167-185.

Chen, S. (2000). Global Comparisons of Earthquake Source Spectra. (Doctor of Philosophy), Carleton University, Ottawa, Ontario, Canada.

Cheng, J., Y. Rong, H. Magistrale, G. Chen, and X. Xu (2019). Earthquake Rupture Scaling Relations for Mainland China, Seismol. Res. Lett. 91, 248-261.

Chiu, H.-C. (1997). Stable baseline correction of digital strong-motion data, Bull. Seismol. Soc. Am. **87**, 932-944.

Chopra, A. K. (2007). Dynamics of structures Theory and applications to earthquake engineering (Third ed., pp. 171-173). New Jersy: Pearson Education Inc.

Goulet, C. A., Kishida, T., Ancheta, T. D., Cramer, C. H., Darragh, R. B., & Silva, W. J. (2014). PEER NGA-East Database. Retrieved from Pacific Earthquake Engineering Research Center.

Graizer, V. M. (1979). Determination of the true ground displacement by using strong motion records, Izv. USSR Acad. Sci., Physics Solid Earth. **15**, 8-885.

Hanks, T. C., & Kanamori, H. (1979). A moment magnitude scale. J. Geophys.Res, 84(B5), 2348-2350.

Hanks, T. C., & McGuire, R. K. (1981). The Character of High-frequency Strong Ground Motion. Bull. Seism. Soc. Am., 71, 2071-2095.

Jiang, W. (2010). Correction method for digital strong motion acceleration records in near-field. Institute of Engineering Mechanics, China Earthquake Administration. Msc. Thesis, 74 pp (in Chinese).

Joshi, A., Kumar, B., Sinvhal, A., & Sinvhal, H. (1999). Generation of synthetic accelerograms by modelling of rupture plane. Journal of Earthquake Technology, 36(1), 43-60.

Kumar, K., S. Thingbaijam, P. M. Mai, and K. Goda (2017). New Empirical Earthquake Source-Scaling Laws, Bull. Seismol. Soc. Am. 107(5), 2225-2246.

Lam, N. T. K., Wilson, J., & Hutchinson, G. (2000). Generation of Synthetic Earthquake Accelerograms Using Seismological Modelling: A Review. Journal of Earthquake Engineering, 4(3), 321-354.

Leonard, M. (2010). Earthquake Fault Scaling: Self-Consistent Relating of Rupture Length, Width, Average Displacement, and Moment Release, Bull. Seismol. Soc. Am. 100(5A), 1971-1988.

Motazedian, D., & Atkinson, G. M. (2005). Stochastic Finite-Fault Modeling Based on a Dynamic Corner Frequency. Bull. Seismol. Soc. Am., 95(3), 995-1010.

Papazafeiropoulos, G. and V. Plevris (2018). OpenSeismoMatlab: A new open-source software for strong ground motion data processing, Heliyon. 4(e00784), 1-39.

Robinson, D., Dhu, T., & Schneider, J. F. (2006). SUA: A computer program to compute regolith site-response and estimate uncertainty for probabilistic seismic hazard analyses. Computers & Geosciences, 32, 109-123.

Silva, W., Gregor, N., & Darragh, R. (2002). Development of Regional Hard Rock Attenuation Relations for Central and Eastern North America. Report to Pacific Engineering and Analysis.

Tang, Y. (2019). Seismic Hazard Analysis and Management for Low-to-moderate Seismicity Regions Based on Ground Motion Simulation. Ph.D. Thesis, The University of Melbourne, Melbourne, Victoria, Australia.

Tang, Y. (2022a). An Updated Corner-frequency Model for Stochastic Finite-fault Ground Motion Simulation, Bull. Seismol. Soc. Am. xx, 1–18, doi: 10.1785/0120210205.

Tang, Y. (2022b). GMSS2.0: An Enhanced Software Program for Stochastic Finite-fault Ground Motion Simulation, Seismol. Res. Lett. xx, 1–12, doi: 10.1785/0220210228.

Tang, Y., Lam, N. T. K., Tsang, H. H., & Lumantarna, E. (2019). Use of Macro-seismic Intensity Data to Validate a Regionally Adjustable Ground Motion Prediction Model. Geosciences, 9(10), 1-22. doi:http://doi.org/10.3390/geosciences9100422

Tang, Y., Lam, N. T. K., Tsang, H. H., & Lumantarna, E. (2020). An Adaptive Ground Motion Prediction Equation for Use in Low-to-moderate Seismicity Regions. Journal of Earthquake Engineering, https://doi.org/10.1080/13632469.2020.1784810.

Tang, Y., N. T. K. Lam, H. H. Tsang (2021). A Computational Tool for Ground Motion Simulations Incorporating Regional Crustal Conditions, Seismol. Res. Lett. 92(2A), 1129-1140.

Tang, Y., X. Xiang, J. Sun, Y. Zhang (2020). A Generic Shear-wave Velocity Profiling Model for Use in Ground Motion Simulations, Geosciences. 10(10), 408.

Wells, D. L. and K. J. Coppersmith (1994). New Empirical Relationships among Magnitude, Rupture Length, Rupture Width, Rupture Area, and surface displacement, Bull. Seismol. Soc. Am. 84(2), 974-1002.

Yenier, E., & Atkinson, G. M. (2014). Equivalent Point-Source Modeling of Moderate-to-Large Magnitude Earthquakes and Associated Ground-Motion Saturation Effects. Bull. Seismol. Soc. Am., 104(3), 1458-1478.

Yenier, E., & Atkinson, G. M. (2015). Regionally Adjustable Generic Ground-Motion Prediction Equation Based on Equivalent Point-Source Simulations: Application to Central and Eastern North America. Bull. Seismol. Soc. Am., 105(4), 1989-2009.

Zeng, Y., Anderson, J., & Yu, G. (1994). A composite source model for computing realistic synthetic strong ground motions. Geophys. Res. Lett., 21, 725-728.